NRC·CNRC

NRC Publications Archive
Archives des publications du CNRC

Mechanical property mapping of cold sprayed Ti splats and coatings

Goldbaum, Dina; Chromik, Richard R.; Yue, Stephen; Irissou, Eric; Legoux, Jean-Gabriel

This publication could be one of several versions: author's original, accepted manuscript or the publisher's version. / La version de cette publication peut être l'une des suivantes : la version prépublication de l'auteur, la version acceptée du manuscrit ou la version de l'éditeur.
For the publisher's version, please access the DOI link below./ Pour consulter la version de l'éditeur, utilisez le lien DOI ci-dessous.

Publisher's version / Version de l'éditeur:
https://doi.org/10.1007/s11666-010-9546-4
Journal of Thermal Spray Technology, 20, 3, pp. 486-496, 2010-12-01

NRC Publications Record / Notice d'Archives des publications de CNRC:
https://nrc-publications.canada.ca/eng/view/object/?id=2f7a4990-3903-454f-a4f7-8b9e0c7e2be4
https://publications-cnrc.canada.ca/fra/voir/objet/?id=2f7a4990-3903-454f-a4f7-8b9e0c7e2be4

Access and use of this website and the material on it are subject to the Terms and Conditions set forth at https://nrc-publications.canada.ca/eng/copyright
READ THESE TERMS AND CONDITIONS CAREFULLY BEFORE USING THIS WEBSITE.

L'accès à ce site Web et l'utilisation de son contenu sont assujettis aux conditions présentées dans le site https://publications-cnrc.canada.ca/fra/droits
LISEZ CES CONDITIONS ATTENTIVEMENT AVANT D'UTILISER CE SITE WEB.

Questions? Contact the NRC Publications Archive team at PublicationsArchive-ArchivesPublications@nrc-cnrc.gc.ca. If you wish to email the authors directly, please see the first page of the publication for their contact information.

Vous avez des questions? Nous pouvons vous aider. Pour communiquer directement avec un auteur, consultez la première page de la revue dans laquelle son article a été publié afin de trouver ses coordonnées. Si vous n'arrivez pas à les repérer, communiquez avec nous à PublicationsArchive-ArchivesPublications@nrc-cnrc.gc.ca.

National Research Council Canada | Conseil national de recherches Canada

Canada

JTTEE5 20:486–496
DOI: 10.1007/s11666-010-9546-4
1059-9630/$19.00 © ASM International

Peer Reviewed

Mechanical Property Mapping of Cold Sprayed Ti Splats and Coatings

Dina Goldbaum, Richard R. Chromik, Stephen Yue, Eric Irissou, and Jean-Gabriel Legoux

(Submitted April 15, 2010; in revised form August 1, 2010)

Profile nanoindentation and nanoindentation mapping were used to investigate the mechanical properties of commercially pure cold spray Ti splats and coatings deposited at increasing deposition velocities. Three regions in the cold spray Ti splats have been indentified: the impact region, the jetting region, and the upper splat region. The mechanical properties measured in these regions were tied to the cold spray deposition process with help of optical and scanning electron microscopes. The jetting region was observed to contribute to a metallurgical bonding of cold spray splats to cold spray splats and was measured to have low hardness in comparison to the splat impact site and similar to the hardness in the upper splat region. No increase in the profile coatings hardness with increase in the particle in-flight velocity and coating thickness was found. A correlation between the mechanical properties and the presently known deposition temperature, stress and dislocation density models was made.

Keywords cold spray, hardness mapping, nanoindentation, titanium

1. Introduction

Cold spray is an emerging coating deposition process (Ref 1) that is carried out at relatively low-temperature condition (Ref 2, 3). The deposition is achieved by powder acceleration to supersonic velocities. Upon the particle impact, the material undergoes plastic deformation which initially results in a conformal material adhesion (Ref 3). At high enough deposition velocities, the particles undergo adiabatic shear instability where a localized fluctuation in the pressure and strain rate leads to a localized rise in the material temperature followed by the material jetting (Ref 4-8).

Much of the current understanding of the cold spray process has been garnered by experimentation and modeling of the deposition of Cu (Ref 5, 7-12). Significant interest is placed on the temperature rise near the impact site and especially in the jetting region as this can have a profound effect on the final microstructure of cold spray coatings. For Cu, a temperature rise of up to 1200 K was estimated for the particle impacting at the deposition velocity of 600 m/s (Ref 4). While the volume of research on Ti is less, similar studies revealed details of the interface phenomenon for this material (Ref 13-22). Zahiri et al. (Ref 14) as well as Vlcek et al. (Ref 19) reported a metallurgical material bonding that was observed in the jetting region in cold sprayed Ti. Also, Zahiri et al. (Ref 14) believed that high-temperature fluctuations induced material softening and grain recrystallization with preferential grain orientation in Ti cold spray splats. Using transmission electron microscopy, Kim, et al. showed both regions of high dislocation density at the impact site of the splat with the substrate (Ref 23) and regions of recrystallization (Ref 24). Thus, a complex and varied microstructure is observed in cold sprayed Ti that may also result in a variation in local mechanical properties.

In this study, the hardness mapping of cold sprayed Ti splats and coatings was used to investigate the presence or lack of thermal softening, which could be associated with material melting in the jetting region. The work carried out is based on a nanoindentation mapping of individual Ti cold sprayed particles deposited at various deposition velocity conditions. The variation in mechanical properties within individual cold spray splats and also within coatings was determined. Nanoindentation technique was used to provide a better understanding of the deposition mechanisms of cold spray Ti splats deposited at various deposition velocity conditions. The effect of the deposition velocity conditions on the mechanical properties of the coatings was investigated.

2. Experimental Procedure

2.1 Sample Preparation

Cold Spray deposition was carried out with a Kinetic 4000 cold spray gun (CGT GmbH, Ampfing, Germany). Nitrogen gas was used as the propelling gas and was pressurized from 2 to 4 MPa and preheated to temperatures ranging from 300 to 800 °C. Feedstock powders were introduced into the cold spray gun and passed through a

Dina Goldbaum, Richard R. Chromik, and **Stephen Yue**, Department of Mining and Materials Engineering, McGill University, 3610 University Street, Montreal, QC H3A 2B2, Canada; and **Eric Irissou** and **Jean-Gabriel Legoux**, National Research Council Canada, Industrial Materials Institute, 75 de Mortagne Blvd, Boucherville, QC J4B 6Y4, Canada. Contact e-mail: richard.chromik@mcgill.ca.

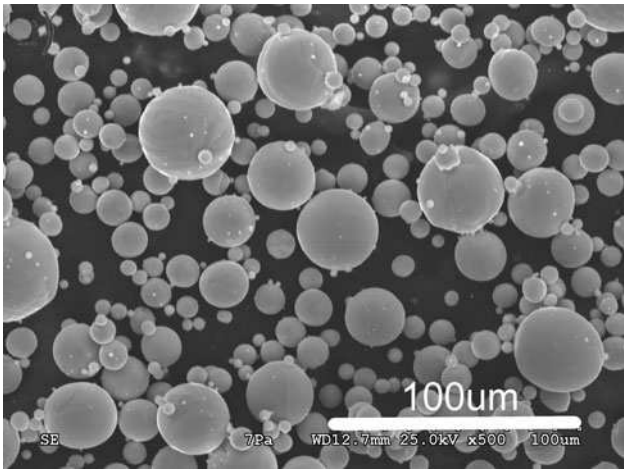

Fig. 1 Micrograph (SEM) of the CP Ti powder used in this study

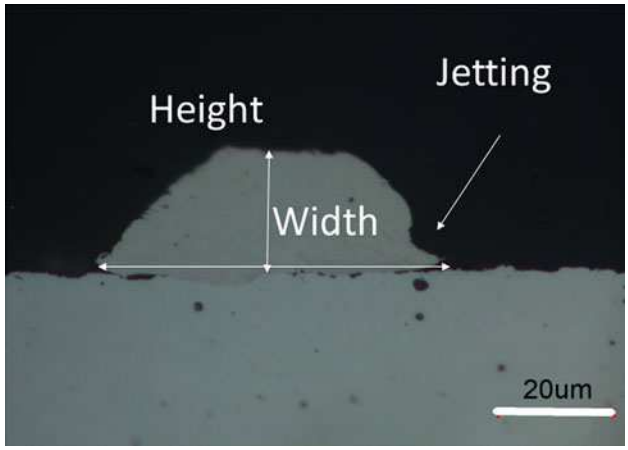

Fig. 2 Micrograph of the cross-section of a Ti splat obtained by LOM. The flattening ratio was measured from images such as these to examine the extent of deformation of Ti splats as a function of deposition velocity

deLeval nozzle (MOC24, CGT, GmbH, Ampfing, Germany), reaching in-flight particle velocities between 580 and 825 m/s. The particle velocity was measured in free jet at various process conditions with a DPV2000 (Tecnar Automation, St-Bruno, QC, Canada) in cold particle mode using a laser diode to illuminate the in-flight particles. The deposition efficiency was measured by taking the ratio of the weight of the deposited coating over the weight of the cold sprayed powder.

The feedstock powder was commercially pure titanium produced by plasma atomization (Raymore Industries, Inc., Boisbriand, QC, Canada). The Ti particles had a spherical morphology (see Fig. 1) and an average particle diameter of 29 μm. The powder size distribution and powder microstructure were reported in a previous publication (Ref 22).

The cold spray gun was mounted onto an automated robotic arm, making possible a wide range of gun motions. Two types of samples were produced by changing the gun's traverse speed and powder feeding rate. For deposition of coatings, the powder feeding rate was 20 g/min and the gun traverse speed was kept at 0.33 m/s. Sixteen coating layers were deposited on one line, on top of the 7.62 × 7.62 × 0.32 cm thick mild steel substrate. Single splats were deposited on mild steel by changing the gun traverse speed to 1.0 m/s and by decreasing the powder feeding rate to 2.0-5.0 g/min. A third type of sample, multi-pass splats, was produced by increasing the number of gun passes over the substrate surface.

2.2 Microstructural Characterization

Cold spray splats were examined both in plan view and in cross-section by scanning electron microscopy (SEM) and light optical microscopy (LOM). For cross-section examination, specimens were mounted in a cold-mount epoxy. The mounted specimens were prepared with metallographic techniques recommended for electron backscatter diffraction (EBSD), which are designed to minimize residual stresses induced by polishing damage. The final polishing step was 0.05 μm colloidal silica. No chemical etching was carried out to minimize surface roughness. The cold spray coatings were prepared in the same manner, first being cut across the coating cross-section (perpendicular to the gun traverse direction). SEM imaging was conducted in a variable pressure scanning electron microscope (Hitachi S-3000 N VP-SEM, Japan).

Image analysis of SEM and LOM micrographs of cold spray splats and coatings was carried out with commercially available image analysis software (Clemex Vision Professional 5.0, Clemex Technology Inc., Longueuil, QC, Canada). LOM micrographs were used to measure the splat flattening ratio, FR, by taking a ratio of splat width to splat height (Ref 7, 25) as shown in Fig. 2. For each deposition conditions, the flattening ratio of between five and twenty-eight splats was measured. The coating porosity was measured from SEM micrographs obtained with the instrument in backscattered imaging mode at 200× magnification. Over three micrographs were analyzed and the average of the measurements with a standard deviation was taken. While porosity measurements quoted here are from SEM micrographs, measurements conducted with LOM micrographs yielded similar results.

2.3 Nanoindentation Testing

The nanoindentation testing was carried out with a diamond Berkovich tip at a maximum load of 1 mN with loading and unloading rate of 200 μN/s and a hold time of 1 s. For coatings, profile indentation was carried out with Ubi 3 nanoindentation system (Hysitron Incorporated, Minneapolis, MN, USA). A total of 20-40 indents per coating at 20-40 μm indent spacing were performed across the center of the coating thickness cross-section. For feedstock powders, splats and multi-pass splats, nanoindentation mapping was conducted with a Triboindenter (Hysitron Inc., Minneapolis, MN, USA) by indenting a matrix of over 100 indents with lateral (x-y) indent spacing of 2.5-3.0 μm. Data analysis and graphing software

(Origin 8.1, OriginLab Corp., Northampton, MA) was used to reconstruct the hardness and reduced modulus distribution in terms of a color scale (i.e., maps of hardness and modulus).

The hardness and elastic modulus of the materials were calculated from the unloading curves using the Oliver and Pharr method (Ref 26). The method is based on the analysis of the unloading curve (load versus displacement) obtained during sample indentation with a calibrated indenter. For studies presented here, both the machine compliance and the tip area function were determined from indentation on a fused quartz standard.

The material hardness was calculated from Eq. 1, where P is the maximum load applied by the tip and A_c is the contact area of the tip.

$$H = \frac{P}{A_c} \quad \text{(Eq 1)}$$

The slope, dP/dh, of the unloading segment defines the material stiffness, S, as well as the reduced elastic modulus, E_r (Ref 26, 27).

$$S = \frac{dP}{dh} = \frac{2E_r\sqrt{A_c}}{\sqrt{\pi}} \quad \text{(Eq 2)}$$

The contact area, A_c, in Eqs. 1 and 2 was determined from the calibrated area function of the tip and a contact depth determined from the Sneddon relationship used as part of the Oliver and Pharr analysis (Ref 26).

The reduced elastic modulus consists of an inverse of the sum of Poisson ratios of the material, υ_m, and indenter, υ_i, divided by their respective elastic modulus, E_m and E_i,

$$E_r = \left[\left(\frac{1-\upsilon_i^2}{E_i}\right) + \left(\frac{1-\upsilon_m^2}{E_m}\right)\right]^{-1} \quad \text{(Eq 3)}$$

With the indenter being diamond ($E_i = 1120$ GPa and $\upsilon_i = 0.07$) and the tested material being Ti ($\upsilon_m = 0.33$), one finds that the Young's modulus of the tested material, E_m is nearly identical to the reduced modulus, E_r. For example, if $E_r = 100$ GPa, $E_m = 102$ GPa. The difference between these two values is much less than the standard deviation on the nanoindentation measurements for E_r. All the values for modulus reported in this article are reduced modulus. Trends or differences in reduced modulus directly reflect trends or differences in the test material's Young's modulus.

3. Results and Discussion

3.1 Microstructure of Cold Sprayed Splats

The appearance of cold spray splats was found to vary as a function of deposition velocity, revealing features distinctive to the deposition mechanisms. Representative SEM images of splats deposited at velocities between 579 and 825 m/s (see Fig. 3) all showed material jetting, indicating the presence of adiabatic shear instability (Ref 4). However, the jetting phenomenon increased with increase in the splat deposition velocity.

The increase in material deformation and material jetting with deposition velocity was further revealed by examination of splat cross-sections (see Fig. 4a-c). As deposition velocity increases, the flattening ratio increases (see Fig. 4d). For a nondeformed powder particle the flattening ratio is 1. The flattening ratio of the splats deposited over a range of 570 to 825 m/s increases from 1.8 to 4. The increase from 1 to 1.8 appears to be largely due to material deformation upon impact (minimal jetting at lower velocities), while the increase from 1.8 to 4 seems to be primarily associated with an increase in material jetting. Aside from material jetting other interesting features were observed that were due to the interaction of Ti particles. At a deposition velocity of 636 m/s (see Fig. 5), a crater formation can be seen at the impact site of the splat. The impact of the splats resulted in a plastic deformation in shape of the impacted body, typical of deformation contributing to a conformal splat adhesion mechanism. While there is also material jetting evident for this splat, the splat has pulled away and partially de-bonded. At higher deposition velocities, this de-bonding was not as pronounced. In Fig. 6, a splat deposited at 770 m/s also appears to have partially pulled away. However, in this case, a region where the jetting region remains attached is observed. While impact angle and location of impact has an effect on these observations, with increasing deposition velocity, the number of events resembling Fig. 6 generally increased and the number of events resembling Fig. 5 decreased. Thus, the increase in jetting with deposition velocity was a significant mechanism for bonding of particles in multi-pass splats.

At higher deposition velocity conditions, the jetting phenomenon becomes more pronounced and evidence of stronger splat adhesion is observed. Figure 6 shows a Ti splat deposited on a previously deposited Ti splat at the deposition velocity of 770 m/s. The close up of the splat shows a continuous bond between two splats in jetting region which could point to a formation of the metallurgical bond in that region (Ref 20).

3.2 Microstructure of Cold Sprayed Ti Coatings

Figure 7 shows cross-sectional images of three Ti coatings that were produced at deposition velocities of 642, 724, and 825 m/s. The coating thickness ranged from 0.9 to 1.4 mm. The coating porosity decreases with increase in the deposition velocity and dense coatings with porosity below 2% are produced at deposition velocity above 724 m/s. Figure 8(a) shows the effect of the deposition velocity on the Ti coating porosity. The deposition efficiency of the coatings increases with increase in the deposition velocity and reaches 100% above the deposition velocity of 725 m/s. The transition coincides with the increase in the flattening ratio observed in Fig. 4.

The coatings discussed in this article consist of single line coatings where the particle impact angle is different from standard multi-line coatings. Some differences in coating porosity measurements and deposition efficiency are expected between coatings produced here and those produced at similar conditions, but as multi-line coatings

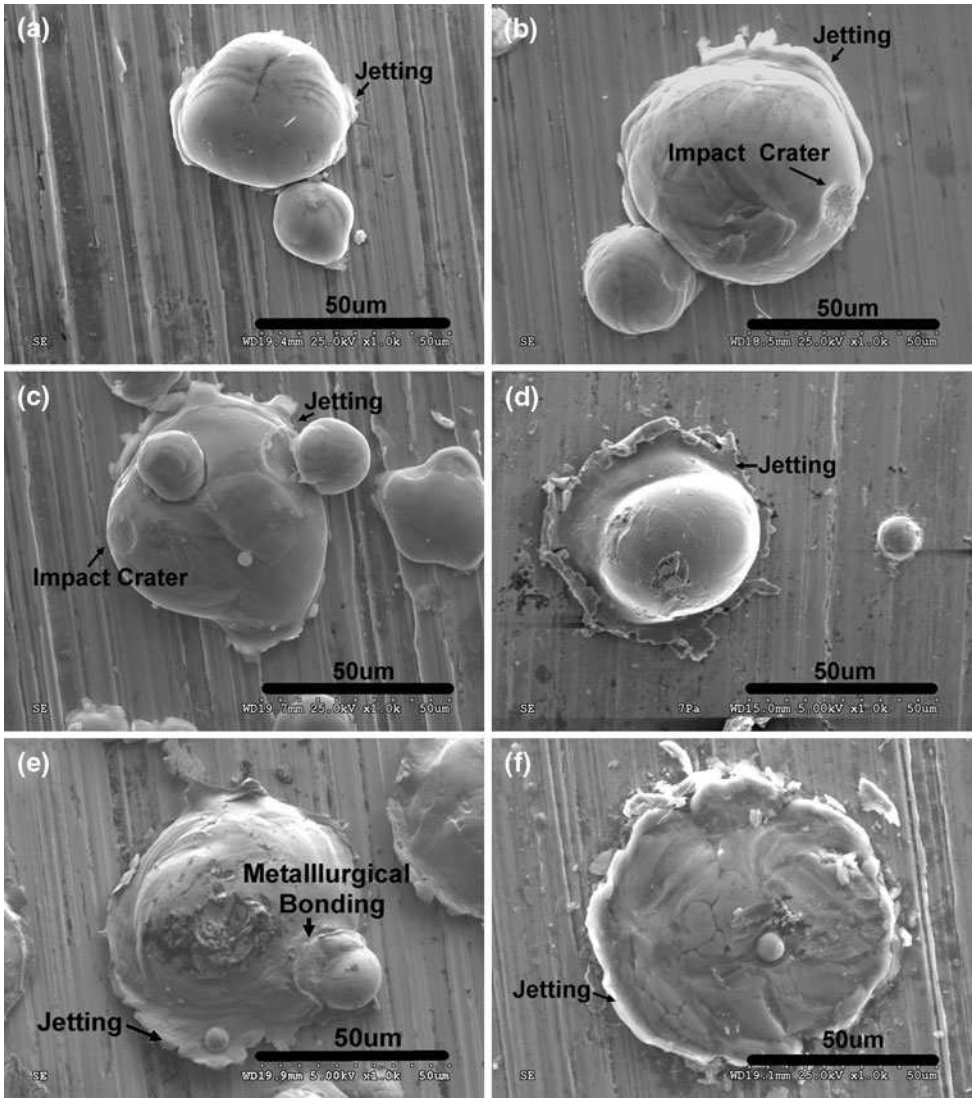

Fig. 3 Micrographs (SEM) of CP Ti splats deposited at: (a) 300 °C, 2 MPa (580 m/s), (b) 300 °C, 4 MPa (642 m/s), (c) 500 °C, 2 MPa (636 m/s), (d) 500 °C, 4 MPa (724 m/s), (e) 750 °C, 3 MPa (770 m/s), and (f) 800 °C, 4 MPa (825 m/s) gas preheat temperature, gas pressure and particle velocity

(Ref 22). Single line coatings were chosen for this study because the particle jet center was easily connected to the center of the coating cross-section, avoiding any concerns over variation of velocity within the jet affecting our measurements (Ref 2).

3.3 Nanoindentation Mapping of Cold Sprayed Splats and Multi-Pass Splats

Mechanical property mapping was carried out on the cold spray Ti splats and feedstock Ti powder. Figure 9 depicts the distribution of hardness and modulus of feedstock Ti powder and cold spray splats deposited at 642, 724, and 825 m/s. The color notation is interpolated between the measurements from indented data points. The color scale has a gradient of 0.2 GPa for hardness and 10 GPa for modulus. The upper and lower limits of the hardness and modulus color scale are annotated by gray and black, while white indicates missing data points. In Fig. 9, black regions represent the measurements made in the epoxy which has low hardness, below 2.2 GPa, and modulus, below 80 GPa. The regions in gray can be found in the mild steel substrate that has a higher elastic modulus when compared to titanium. For comparison, the optical images of the indented cold spray splats are shown at the left-hand side of Fig. 9.

Nanoindentation maps reveal that the hardness distribution inside of the cold spray splats or feedstock powder is not homogeneous (see Fig. 9). In the feedstock powder, high hardness of 3.6 to 3.8 GPa is measured at the powder outer surface layer. A martensitic microstructure was often observed in this region, possibly a result of surface tension during the powder production through a plasma atomization process. However, in splats,

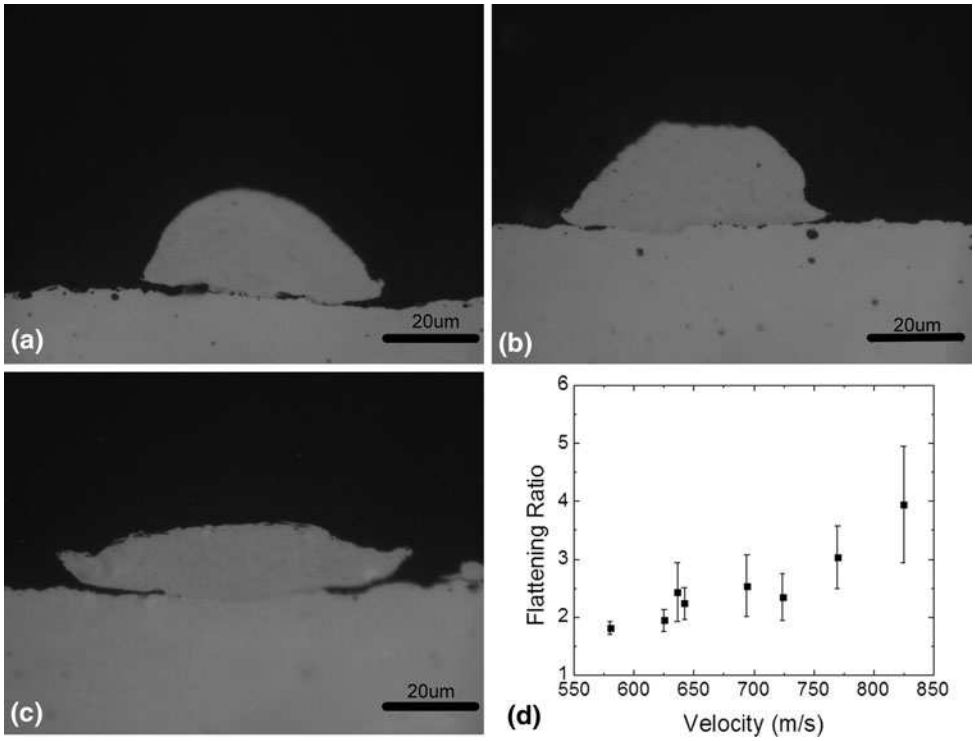

Fig. 4 Micrographs (LOM) of Ti splat cross-section deposited at (a) 300 °C, 4 MPa (642 m/s), (b) 500 °C, 4 MPa (724 m/s), (c) 800 °C, 4 MPa (825 m/s) gas preheat temperature, gas pressure, and particle velocity, and (d) the flattening ratio with standard deviation of Ti splats with respect to the deposition velocity

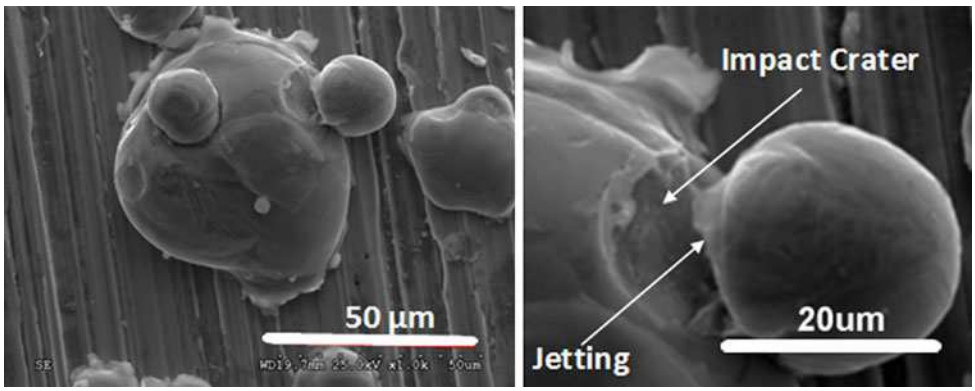

Fig. 5 Micrographs (SEM) of splat deposited at 500 °C, 2 MPa (636 m/s) and demonstrating a conformal particle adhesion

high hardness regions are mainly observed at the splat impact site with the substrate material. The hardness in these regions reaches 4.2 GPa and is color coded in red. Relatively lower hardness of 3.0-3.4 GPa is measured in the upper splat portion.

In Table 1, the average hardness and modulus of the splats have been calculated. The average splat hardness does not increase significantly with increase in the deposition velocity. The splats hardness is, however, higher than that of the feedstock powder. The modulus of the single splats is similar to the modulus of the feedstock powder. The residual stresses induced by impact are expected to cause an increase in hardness but have little effect on the elastic properties.

As opposed to the single pass splats, multi-pass splats showed a higher modulus. In Fig. 10, modulus of 120 GPa and higher is measured in the splats deposited above 500 °C gas preheat temperature. As the gas preheat temperature increases to 800 °C, the modulus of the splats increases up to 130 GPa. These values of the modulus are consistent with that of Ti, and could simply be an effect of differences in crystallographic texture.

In multi-pass splats, higher hardness is found both at the impact site between splats and near the steel substrate.

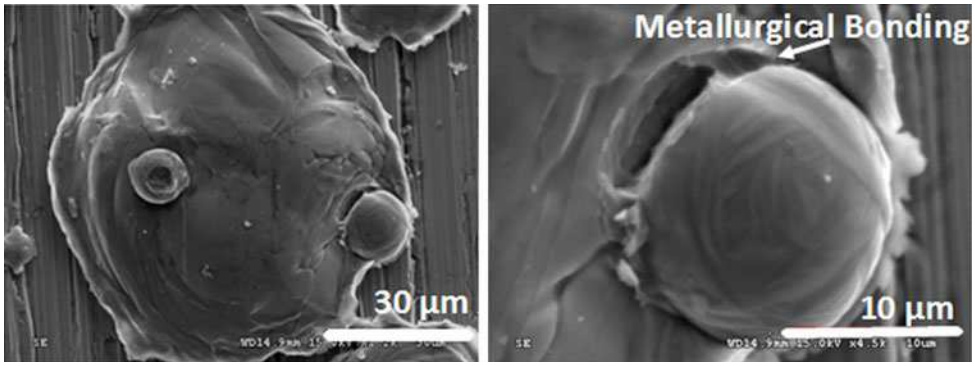

Fig. 6 Micrographs (SEM) showing ductile fracture in the jetting region of CP Ti splat deposited at 750 °C, 3 MPa (770 m/s)

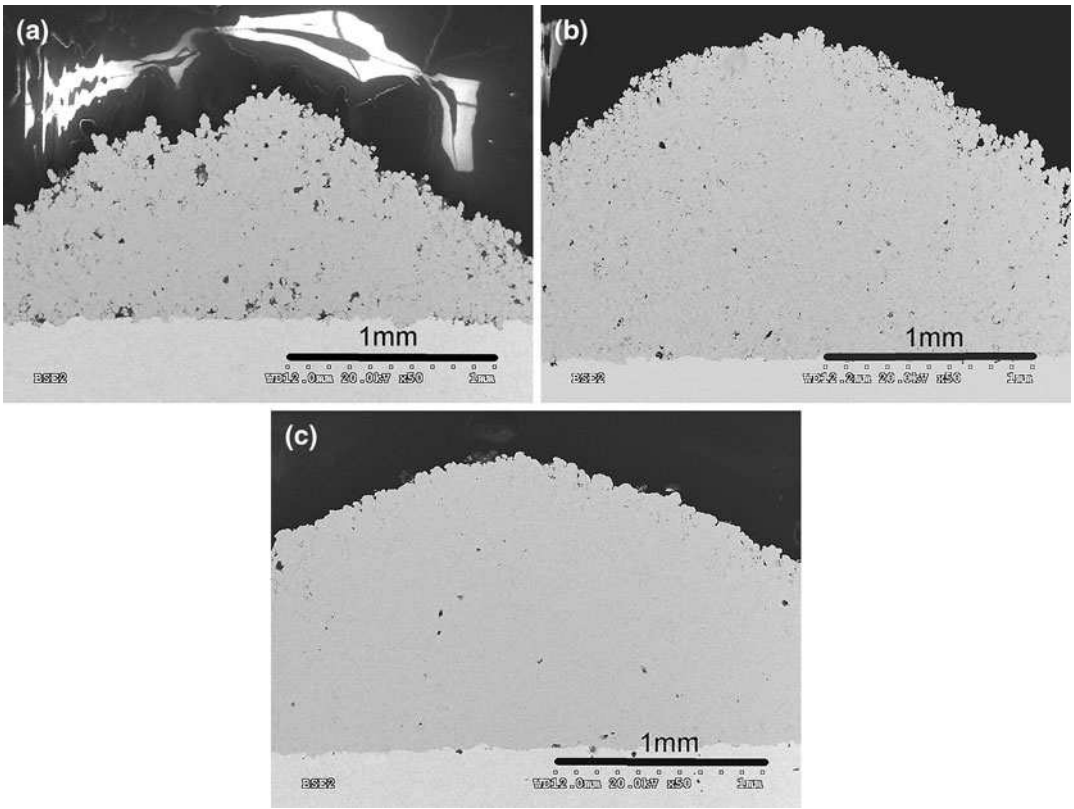

Fig. 7 Micrographs (SEM) of cold spray Ti coatings deposited at: (a) 300 °C, 4 MPa (642 m/s), (b) 500 °C, 4 MPa (724 m/s), and (c) 800 °C, 4 MPa (825 m/s)

In Fig. 10, multi-pass titanium splats deposited at 642, 724, and 825 m/s are shown along with hardness and modulus maps. Regions of 3.7-4.2 GPa hardness were measured in the impact region between two splats as well as in the impact region of the splat on the steel substrate. However, in the jetting region, a lower hardness of 3.2-3.4 GPa was measured for the 825 m/s splat.

3.4 Nanoindentation of Cold Sprayed Ti Coatings

Profile nanoindentation across cold spray Ti coatings revealed that the mechanical properties of these cold spray coatings did not change with the coating thickness. A typical profile of hardness and modulus measured across coating thickness cross-section is shown in Fig. 11(a) for a coating deposited at 500 °C gas preheat temperature, 4 MPa gas pressure, and 724 m/s particle deposition velocity. Similar trends were observed for all coatings produced at all deposition velocity conditions. This result is contrary to previously published results for microindentation on cold sprayed titanium (Ref 11, 22) where the hardness was seen to increase near the substrate/coating interface due to a tamping effect. This difference is likely due to the effect porosity and particle

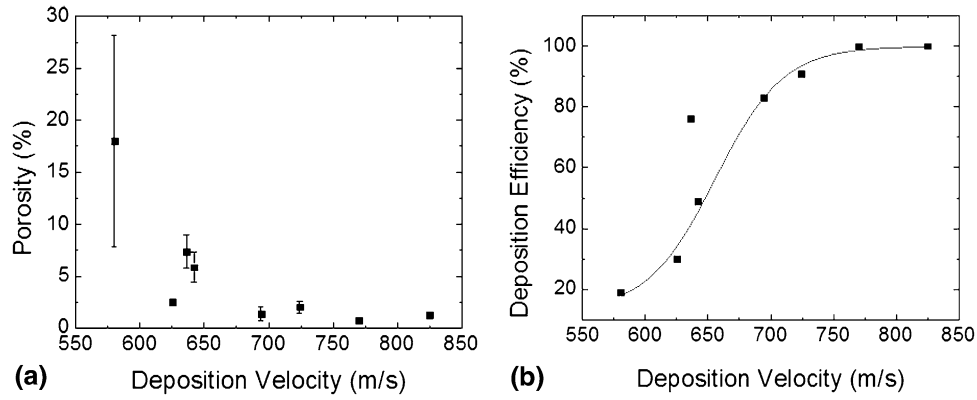

Fig. 8 Graphs of (a) porosity with a standard deviation and (b) deposition efficiency of cold spray Ti coatings vs. deposition velocity

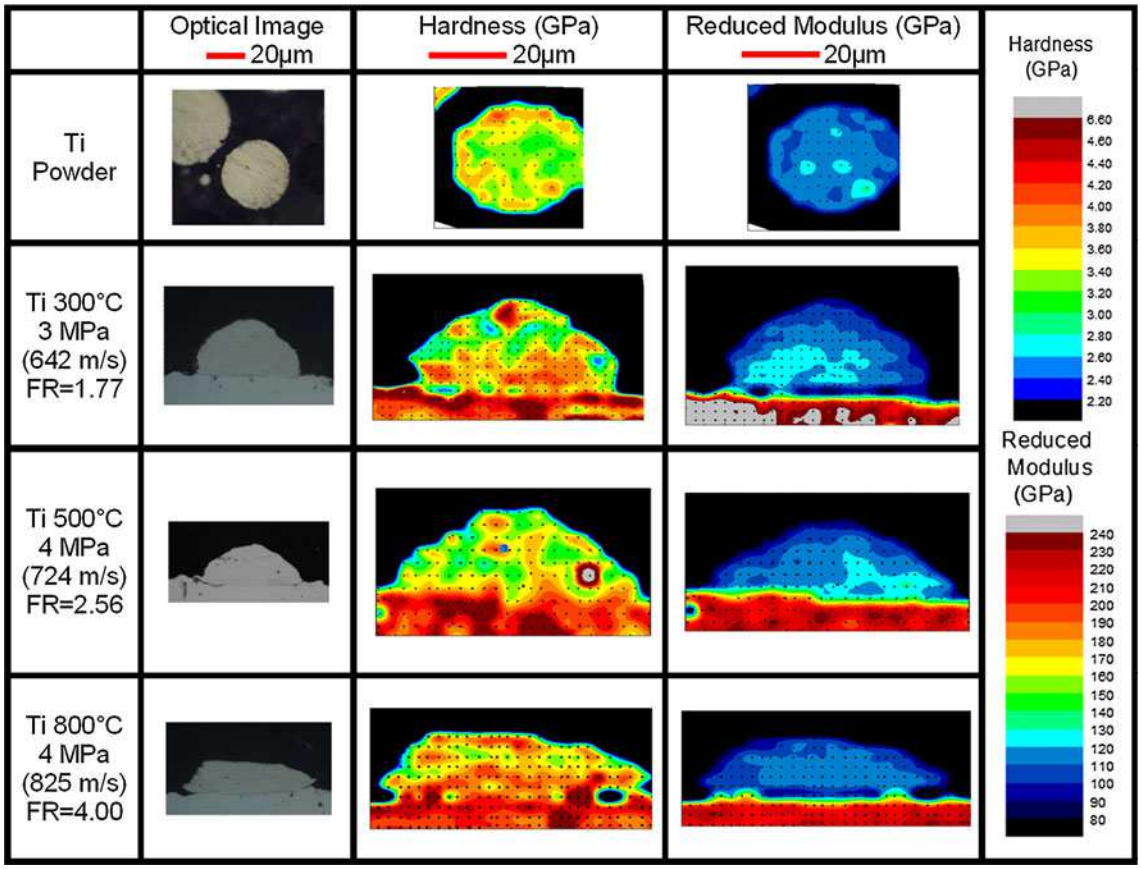

Fig. 9 Hardness and modulus maps of Ti powder for Ti splats deposited at: 300 °C, 3 MPa (642 m/s); at 500 °C, 4 MPa (724 m/s), and at 800 °C, 4 MPa (825 m/s). Micrographs (LOM) of the splats and powder are provided on the left-hand side. The hardness and modulus color scale bars are provided at the right-hand side with black demonstrating lower end values and gray showing higher end values

de-bonding has on the hardness test. Nanoindentation is affected the least and represents mechanical properties of the cold sprayed material, while microindentation provides a measure of the overall mechanical response of the coating, including defects.

The average hardness and modulus from profile indentation is plotted against the deposition velocity in Fig. 11(b), with the mechanical properties of the feedstock Ti powder plotted at 0 m/s. Higher hardness and modulus are measured in the cold spray coatings in comparison to the titanium feedstock powder. The hardness and modulus of the coatings deposited above 625 m/s was 3.7 ± 0.2 GPa and 125 ± 10 GPa, respectively. The hardness and modulus of the initial feedstock powder was 3.2 ± 0.2 GPa and 110 ± 5 GPa. No significant change in the coating hardness with increase in the coating deposition velocity

Table 1 Mechanical properties of Ti powder and cold spray Ti coatings and Ti splats

Specimen/conditions	Deposition velocity, m/s	Deposition efficiency, %	Coating porosity, %	Coating hardness, GPa	Coating modulus, GPa	Splat flattening ratio	Splat hardness, GPa	Splat modulus, GPa
Ti powder/as-polished	N/a	N/a	<1	3.1 ± 0.3	107 ± 9	N/a	3.1 ± 0.3	107 ± 9
Ti/300 °C, 2 MPa	580	19	18.0 ± 10.1	3.2 ± 0.3	99 ± 11	1.8 ± 0.1	-	-
Ti/300 °C, 3 MPa	625	30	2.5 ± 0.3	3.6 ± 0.2	112 ± 12	2.0 ± 0.2	3.4 ± 0.4	103 ± 9
Ti/300 °C, 4 MPa	642	49	5.9 ± 1.5	3.7 ± 0.2	116 ± 13	2.2 ± 0.3	-	-
Ti/500 °C, 2 MPa	636	76	7.4 ± 1.6	3.6 ± 0.4	117 ± 10	2.4 ± 0.5	-	-
Ti/500 °C, 3 MPa	694	83	1.4 ± 0.6	3.7 ± 0.3	120 ± 11	2.5 ± 0.5	-	-
Ti/500 °C, 4 MPa	724	91	2.1 ± 0.6	3.5 ± 0.3	109 ± 8	2.3 ± 0.4	3.6 ± 0.4	119 ± 6
Ti/750 °C, 3 MPa	770	100	0.7 ± 0.1	3.7 ± 0.4	120 ± 7	3.0 ± 0.6	-	-
Ti/800 °C, 4 MPa	825	100	1.3 ± 0.3	3.5 ± 0.3	121 ± 6	3.9 ± 1.0	3.7 ± 0.4	110 ± 7

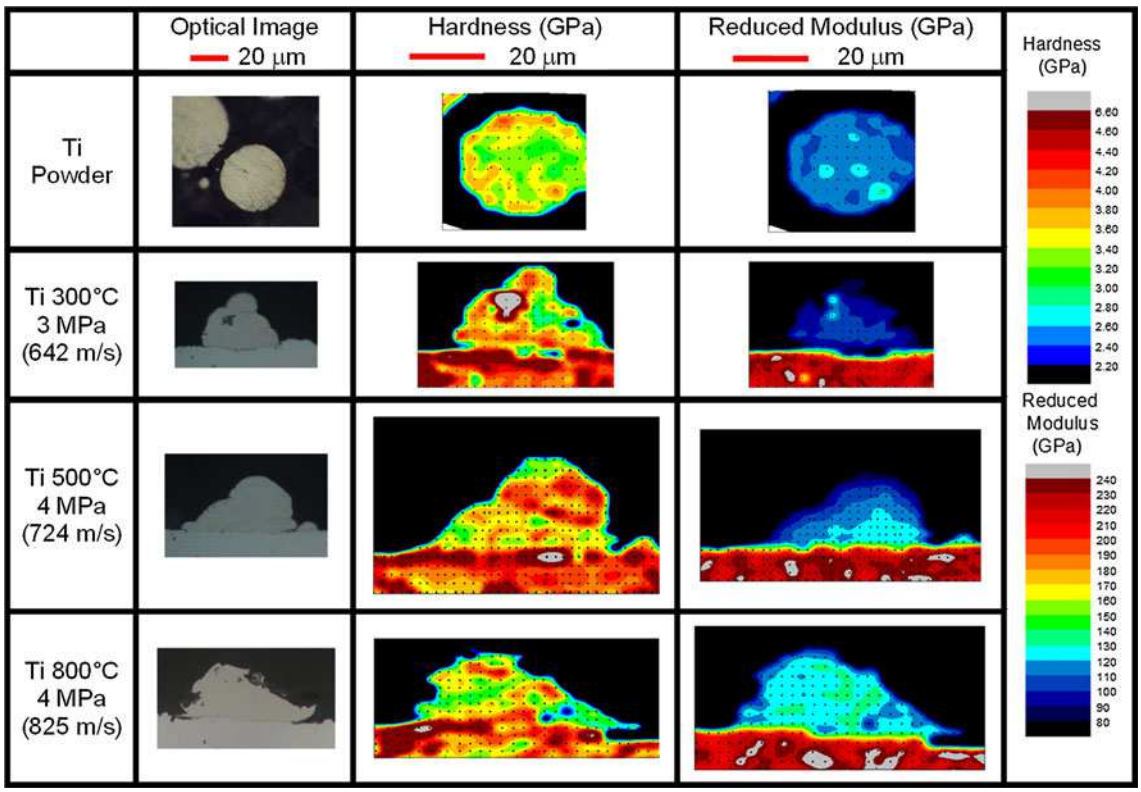

Fig. 10 Hardness and reduced modulus maps of the multi-pass splats deposited at 300 °C, 3 MPa (642 m/s); at 500 °C, 4 MPa (724 m/s), and at 800 °C, 4 MPa (825 m/s). Micrographs (LOM) of the splats and powder are provided on the left-hand side. The hardness and modulus color scale bars are provided at the right-hand side with black demonstrating lower end values and gray showing higher end values

past 650 m/s range was observed. Average hardness and modulus for all the coatings are summarized in Table 1.

It should be noted that mechanical property mapping was also conducted on coatings. Similar small-scale variation in mechanical properties across particle boundaries was also observed. Thus, while the average properties of the cold sprayed coatings do not change over the length scale of the coating thickness, small variations similar to those observed in the splats do exist in the coatings at a similar length scale to the particles.

3.5 Deposition Mechanisms, Mechanical Properties, and Comparisons to Literature

Splat bonding mechanisms, extent of deformation, degree of jetting, and mechanical properties were all observed to vary to greater or lesser degrees as a function of deposition velocity. The relationships between all these phenomena are complex, but the results of this study along with those in the literature leads to the following discussion of the observable trends with deposition velocity.

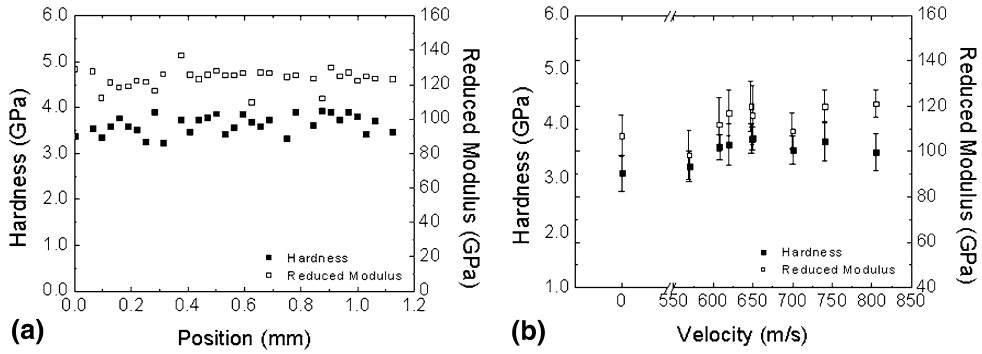

Fig. 11 (a) Nanoindentation profile hardness and modulus of Ti coatings deposited at 500 °C, 4 MPa (724 m/s) away from the coating and the substrate interface plotted at 0 mm, (b) Average profile nanoindentation hardness and modulus with standard deviation of coatings plotted against their respective deposition velocities. For reference, the average properties for the powder are plotted at 0 m/s

When titanium was sprayed at velocities below 725 m/s, the deposition efficiency was below 100% and the flattening ratio of the splats was roughly constant between 1.8 and 2.5. While some material jetting was observed for these splats, it was somewhat minimal compared to those deposited at higher velocities (c.f. Fig. 3, 9). Additionally, evidence of de-bonding of splats (c.f. Fig. 5) indicated that the jetting was in some instances not providing a strong metallurgical bond. Above 725 m/s, the deposition efficiency was 100% and the flattening ratio rose to a value of 3 at 770 m/s and 3.9 at 825 m/s. In this regime, significant jetting occurred and evidence metallurgical bonding was also found (c.f. Fig. 6). These observations, especially the increase in material jetting with particle velocity, are consistent with the current understanding of the mechanism of adiabatic shear instability as a deposition mechanism for cold spray (Ref 4, 6, 7). The transition to 100% deposition efficiency at roughly 725 m/s matches very well the predicted critical velocity of ~700 m/s for 25 μm diameter titanium particles, Schmidt et al. (Ref 4). In terms of mechanical properties, the cold spray splats and coatings are always on average harder than the feedstock Ti powder. However, no significant increase in the coating or splat hardness was measured with the increase in particle velocity. To explore this phenomenon further, we plot the hardness of cold spray splats near the interface and far from the interface as a function of deposition velocity (see Fig. 12). Near interface hardness is generally significantly higher than the feedstock powder, indicating work hardening during the impact. This hardness remains relatively constant with particle velocity, seeming to indicate that the extent of work hardening has reached a maximum in this area even at the lowest velocity. However, as the velocity increases, the hardness far from the interface does increase gradually, perhaps due to some deformation and increased dislocation density in the upper splat regions. Lastly, the hardness of the jetting region is also plotted in Fig. 12 for the splat with the highest deposition velocity of 825 m/s (c.f. Fig. 10). In the jetting region, the hardness is similar to the feedstock powder. Thus, while the average mechanical properties remain constant with deposition velocity, the complex phenomenon of particle impact, deformation and jetting is

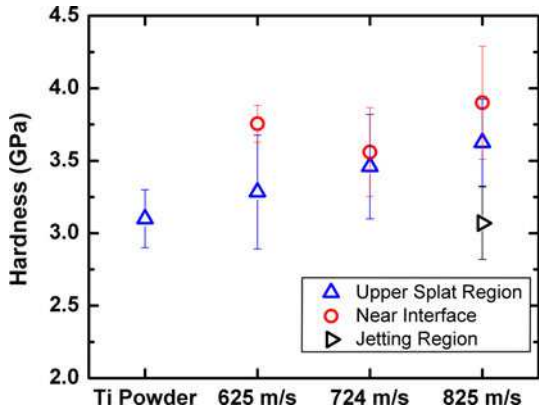

Fig. 12 Hardness distribution with respect to the splat deposition velocity in Ti splat regions: near interface, in the jetting region and in the upper splat region

also evident in the variation of hardness in the different regions of the splats. This discussion and the splat hardness maps correlate well with the dislocation density distribution in the TEM image of Ti splats taken by Kim et al. (Ref 24) and also the simulated stress distribution patterns proposed by Assadi et al. (Ref 7) Thus, there appears to be a consistent picture of high dislocation density and hardness near the interface, minimal activity in the upper splat region, and the possibility of thermal softening in the jetting regions.

According to Kapoor et al., high strain rate deformation of Ti, such as that occurring in the jetting region, can be very efficient at converting deformation work into heat (Ref 25). The temperature rise in the jetting region was estimated to reach near melting point (<90% of T_m) for Ti splats deposited on a steel substrate with nitrogen gas at 950 m/s deposition velocity (Ref 20). Higher temperatures have been estimated for Ti splats deposited on a Ti substrate (Ref 28). The extent to which this heat affects the resulting microstructure and distribution of strain is difficult to predict. Others have shown that the temperature rise during impact of cold sprayed material is sufficient to induce a dynamic recrystallization in the cold spray deposited Ti splats (Ref 24). In addition, there has been

evidence that the recrystallization can result in preferential grain orientation of cold spray Ti coatings (Ref 14). For all splats and coatings studied here, the modulus measured by indentation is within the normal range for Ti, which can vary from 100 to 145 GPa (c.f. Eq. 3). As it is not a pure uniaxial test, indentation is not very sensitive to changes variations due to crystallographic orientation (Ref 29, 30). Thus, the small changes observed in our data may or may not reflect some degree of preferred orientation in the sprayed material.

4. Conclusions

The mechanical properties of cold sprayed Ti splats and coatings were studied by nanoindentation. When compared to the hardness of the feedstock powder, the distribution of hardness within individual Ti cold spray splats demonstrated three regions: (1) an impact site with an increase in hardness, (2) an upper splat region with similar hardness to feedstock material, and (3) jetting regions where the hardness is similar to the feedstock material. At lower deposition velocities (<650 m/s), the first two regions were more evident than the third, indicating primarily conformal adhesion. At higher deposition velocities (>650 m/s), the third region, the jetting region, became more pronounced, indicating the formation adiabatic shear instability. The mechanical properties measured in these three regions are consistent with results in the literature that show increased dislocation density near the interface and dynamic recrystallization in the jetting region. Thus, at the highest deposition velocities, which are preferred due to low coating porosity and high deposition efficiency, there was sufficient heat in the jetting regions to promote dynamic recrystallization in Ti and a reduction in hardness. However, there is retention of work hardening at the impact site away from the jetting region, where there is high strain, but insufficient strain rate to realize a significant temperature rise. Despite the significant differences in hardness in the different regions, the average hardness of cold sprayed Ti splats remained similar for all deposition velocities and was greater than the feedstock material. The same was observed for the cold spray coatings produced, where there were local variations in mechanical properties but the coating mechanical properties remained constant across the coating thickness cross-section.

Acknowledgments

Financial support from the Canadian Foundation for Innovation is gratefully acknowledged; the cold spray equipment was provided by CFI project No. 8246 while the nanoindentation equipment was provided by CFI, Leader's Opportunity Fund, project No. 13029. Operational funding for this project was provided by the Natural Sciences and Engineering Research Council (NSERC) Strategic Grants Program. The authors acknowledge the technical assistance of Ahmad Rezaeian, Bernard Harvey and Frederic Belval.

References

1. E. Irissou, J.G. Legoux, A. Ryabinin, B. Jodoin, and C. Moreau, Review on Cold Spray Process and Technology: Part I, Intellectual Property, *J. Therm. Spray Technol.*, 2008, **17**(4), p 495-516
2. A. Papyrin, V. Kosarev, K. V. Klinkov, A. Alkhimov, and V. M. Fomin, *Cold Spray Technology*, Elsevier, Oxford, 2006, p 74, 153-169, 259
3. V.K. Champagne, *The Cold Spray Materials Deposition Process: Fundamentals and Applications*, Woodhead Publishing Limited, Cambridge, 2007, p 362
4. T. Schmidt, F. Gärtner, H. Assadi, and H. Kreye, Development of a Generalized Parameter Window for Cold Spray Deposition, *Acta Mater.*, 2006, **54**(3), p 729-742
5. C.-J. Li, W.-Y. Li, and H. Liao, Examination of the Critical Velocity for Deposition of Particles in Cold Spraying, *J. Therm. Spray Technol.*, 2006, **15**(2), p 212-222
6. M. Grujicic, C.L. Zhao, W.S. DeRosset, and D. Helfritch, Adiabatic Shear Instability Based Mechanism for Particles/Substrate Bonding in the Cold-Gas Dynamic-Spray Process, *Mater. Des.*, 2004, **25**(8), p 681-688
7. H. Assadi, F. Gärtner, T. Stoltenhoff, and H. Kreye, Bonding Mechanism in Cold Gas Spraying, *Acta Mater.*, 2003, **51**(15), p 4379-4394
8. T. Schmidt, F. Gaertner, and H. Kreye, New Developments in Cold Spray Based on Higher Gas and Particle Temperatures, *J. Therm. Spray Technol.*, 2006, **15**(4), p 488-494
9. C. Borchers, F. Gartner, T. Stoltenhoff, and H. Kreye, Microstructural Bonding Features of Cold Sprayed Face Centered Cubic Metals, *J. Appl. Phys.*, 2004, **96**(8), p 4288-4292
10. T. Kairet, M. Degrez, F. Campana, and J.P. Janssen, Influence of the Powder Size Distribution on the Microstructure of Cold-Sprayed Copper Coatings Studied by X-ray Diffraction, *J. Therm. Spray Technol.*, 2007, **16**(5), p 610-618
11. A. Rezaeian, E. Irissou, R.R. Chromik, S. Yue, Characterization of Cold-Sprayed Ni, Ti, Cu Coating Properties for their Optimization, *Thermal Spray: Crossing Borders*, Jun 2-4, 2008 (Maastricht, The Netherlands), ASM International, p 854-859
12. T.H. Van Steenkiste, J.R. Smith, R.E. Teets, J.J. Moleski, D.W. Gorkiewicz, R.P. Tison, D.R. Marantz, K.A. Kowalsky, W.L. Riggs, P.H. Zajchowski, B. Pilsner, R.C. McCune, and K.J. Barnett, Kinetic Spray Coatings, *Surf. Coat. Technol.*, 1999, **111**(1), p 62-71
13. T. Stoltenhoff, C. Borchers, F. Gärtner, and H. Kreye, Microstructures and Key Properties of Cold-Sprayed and Thermally Sprayed Copper Coatings, *Surf. Coat. Technol.*, 2006, **200**(16-17), p 4947-4960
14. S. Zahiri, D. Fraser, and M. Jahedi, Recrystallization of Cold Spray-Fabricated CP Titanium Structures, *J. Therm. Spray Technol.*, 2009, **18**(1), p 16-22
15. C.-J. Li and W.-Y. Li, Deposition Characteristics of Titanium Coating in Cold Spraying, *Surf. Coat. Technol.*, 2003, **167**(2-3), p 278-283
16. W.Y. Li, C. Zhang, X. Guo, J. Xu, C.J. Li, H. Liao, C. Coddet, and K.A. Khor, Ti and Ti-6Al-4V Coatings by Cold Spraying and Microstructure Modification by Heat Treatment, *Adv. Eng. Mater.*, 2007, **9**(5), p 418-423
17. R.S. Lima, A. Kucuk, C.C. Berndt, J. Karthikeyan, C.M. Kay, and J. Lindemann, Deposition Efficiency, Mechanical Properties and Coating Roughness in Cold-Sprayed Titanium, *J. Mater. Sci. Lett.*, 2002, **21**(21), p 1687-1689
18. T. Marrocco, D. McCartney, P. Shipway, and A. Sturgeon, Production of Titanium Deposits by Cold-Gas Dynamic Spray: Numerical Modeling and Experimental Characterization, *J. Therm. Spray Technol.*, 2006, **15**(2), p 263-272
19. J. Vlcek, H. Huber, H. F. Voggenreiter, and E. Lugscheider, Melting Upon Particle Impact in the Cold Spray Process, *International Congress on Advanced Materials, Their Process and*

Applications, September 30-October 2, 2002 (Munich, Germany), Deutsche Gesellschaff Fur Materialkunde (DSM)
20. G. Bae, S. Kumar, S. Yoon, K. Kang, H. Na, H.J. Kim, and C. Lee, Bonding Features and Associated Mechanisms in Kinetic Sprayed Titanium Coatings, *Acta Mater.*, 2009, **57**(19), p 5654-5666
21. K. Kim, M. Watanabe, K. Mitsuishi, K. Iakoubovskii, and S. Kuroda, Impact Bonding and Rebounding Between Kinetically Sprayed Titanium Particle and Steel Substrate Revealed by High-Resolution Electron Microscopy, *J. Appl. Phys. D*, 2009, **42**(6), p 65304
22. W. Wong, A. Rezaeian, E. Irissou, J.G. Legoux, and S. Yue, Cold Spray Characteristics of Commercially Pure Ti and Ti-6Al-4V, *Adv. Mater. Res.*, 2010, **89-91**, p 639-644
23. K.-H. Kim, M. Watanabe, J. Kawakita, and S. Kuroda, Grain Refinement in a Single Titanium Powder Particle Impacted at High Velocity, *Scripta Mater.*, 2008, **59**(7), p 768-771
24. K.-H. Kim, M. Watanabe, J. Kawakita, and S. Kuroda, Effects of Temperature of In-flight Particles on Bonding and Microstructure in Warm-Sprayed Titanium Deposits, *J. Therm. Spray Technol.*, 2009, **18**(3), p 392-400
25. R. Kapoor and S. Nemat-Nasser, Determination of Temperature Rise During High Strain Rate Deformation, *Mech. Mater.*, 1998, **27**(1), p 1-12
26. A. C. Fisher-Cripps, Nanoindentation, 2nd ed., Springer, New York, 2002, p 1-20
27. W.C. Oliver and G.M. Pharr, Measurement of Hardness and Elastic Modulus by Instrumented Indentation: Advances in Understanding and Refinements to Methodology, *Mater. Res. Soc.*, 2004, **19**(1), p 3-20
28. G. Bae, Y. Xiong, S. Kumar, K. Kang, and C. Lee, General Aspects of Interface Bonding in Kinetic Sprayed Coatings, *Acta Mater.*, 2008, **56**(17), p 4858-4868
29. J.J. Vlassak and W.D. Nix, Measuring the Elastic Properties of Anisotropic Materials by Means of Indentation Experiments, *J. Mech. Phys. Solids*, 1994, **42**(8), p 1223-1245
30. J.J. Vlassak, M. Ciavarella, J.R. Barber, and X. Wang, The Indentation Modulus of Elastically Anisotropic Materials for Indenters of Arbitrary Shape, *J. Mech. Phys. Solids*, 2003, **51**(9), p 1701-1721